Light Metals 2014
Edited by: John Grandfield
TMS (The Minerals, Metals & Materials Society), 2014

PARALLEL LABORATORY AND INDUSTRIAL SCALE ALUMINIUM FILTRATION TESTS WITH Al_2O_3 AND SiC BASED CFF FILTERS

Martin Syvertsen[1], Anne Kvithyld[1], Sarina Bao[1], Arne Nordmark[1], Anders Johansson[2]
[1]SINTEF Materials and Chemistry, Alfred Getz vei 2, NO-7465 Trondheim, Norway
[2]SAPA Heat Transfer AB, S-612 81 Finspång, Sweden

Keywords: Melt treatment, Filtration, Filter material

Abstract

Filtration experiments with Al_2O_3 and SiC based CFF filter types were conducted both in laboratory scale and in industrial scale.

The laboratory scale set-up was designed so that melt with the same inclusion content flowed through the two filter types with the same pressure drop.

The metal flow through each filter was continuously recorded during the experiments. Image analysis was used on the filter cross sections after the filtration test in order to determine difference in filtration efficiency between the two filter types.

The same filter types were also tested in industrial scale experiments. LiMCA II was used to measure the inclusion content in the melt before and after the filters. A recently published method was used to calculate the removal efficiencies in the filters.

Introduction

Earlier work has indicated that different filter material can have different filtration efficiency [1]. It has been suggested that the wetting between the filter material and liquid aluminium can play a role with regard to filtration efficiency [2]. The contact angle of molten aluminium on the pure materials and [3] filter materials [4] was measured in wetting experiments, as shown in Table 1. Figure 1 shows a photograph from a wetting experiment with liquid aluminium on an alumina substrate.

Table 1: Measured wetting angles on the substrates made from the filter materials used in the parallel experiments [4] and pure compounds [3].

	Al_2O_3 filter	SiC filter	pure Al_2O_3	pure SiC
1100°C	84°	39°	61° ± 2°	55°
1200°C	44°	28°	52 °± 5°	30°

Aluminium is readily oxidized even if the oxygen partial pressure is as low as 10^{-44} Pa at 700°C [3]. Such a low oxygen partial pressure is extremely difficult to achieve experimentally. Nevertheless, the oxide layer on the surface of a molten aluminium drop can be removed, if the outgoing flow of gaseous Al_2O is greater than the incoming flow of oxygen. The equilibrium partial pressure of Al_2O is 4.3 Pa at 1000°C. Holding the total pressure in the furnace under 10^{-3} Pa, the oxide skin on the aluminium drop will evaporate. This allows measuring the contact angles between molten aluminium and the solid substrate at temperatures higher than 1000°C.

Hence, two filter materials with different wetting properties have been tested and evaluated. It is assumed that even though the contact angle at 700°C has not been measured, we believe that there also will be a difference in the wetting angles at 700°C and thus the filtration behavior. The results are presented in this paper.

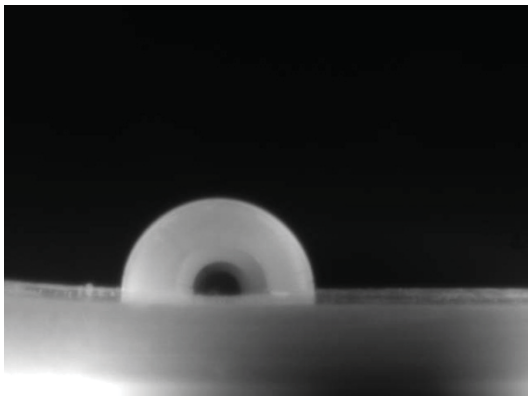

Figure 1: Al on Al_2O_3 filter substrate, 1100°C

Experimental set-up

Two sets of filtration experiments are presented here. The first set shows a laboratory scale set-up where two filter types are tested at the same time under the same conditions. The second set-up is industrial scale where the two filter types are tested on similar batches during casting of rolling billets.

Lab scale experiments

Anodized profiles with oxide thickness from 5 to 15 µm were chosen as test material whereas typical natural oxide is in the order of 10nm [5]. By using anodized material it will be easier to detect the oxide films in the later microscopic image analyses. Therefore, about 150 kg of anodized extruded aluminium profiles were melted in an electrically heated furnace and used for the filtration experiments. The alloy was a mixture of alloys partly AA 6060 and AA 6063.

The melt temperature was held at about 750°C before the metal was stirred with a gas injection impeller for 30 seconds and skimmed. Bi-film index samples [5] were taken from the melt in order to determine the melt quality before each of the filtration experiments was done.

The set-up of the experiments was designed so that melt with the same amount of inclusions, temperature, and metallographic pressure enters the two test-filters in the same way. Sand moulds were designed, and these were made with resin bonded silica sand with an average grain size of 0.15mm. This ensured repeatability in the melt flow pattern before and through the filters.

Figure 2 shows a schematic of the void in the sand mould. The metal is poured into the cup on top and flows down and out into

the two chambers where the filters are positioned (red area). Below the filter is a choke which adjust the metal flow through the filters and secures that the filters are filled with metal during the tests. The temperature of the metal is recorded continuously by thermocouples positioned below the filters. After the metal has run through the filters and out of the choke it flows down into two coated steel pans, each placed on a scale so the metal flow through each filter is also recorded. The metallographic head over the filter was about (300 ± 10) mm during the experiments.

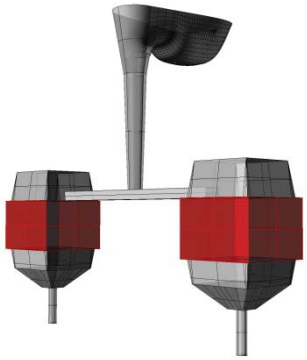

Figure 2: Schematic of the sand mould used for testing two filter types simultaneously.

The Al_2O_3-based and SiC-based filters were produced at Drache in the size of 10"×10". The filters were cut into pieces of 70mm×70mm before testing. They were preheated in an air circulating furnace at 500°C before they were put into the mould and the experiments were done. The composition and characteristics of the two filter types are presented in Table 2.

Table 2: Composition and characteristics of the filters used in the parallel experiments.

	Al_2O_3 based filter		SiC based filter	
Composition [%]	Al_2O_3	85 – 90	Al_2O_3	5 – 9
	P_2O_5	≈ 6	SiC	58 – 64
	SiO_2	≈ 6	SiO_2	29 – 33
	$K_2O + Na_2O$	≈ 1		
Grade [ppi]	30		30	
Measured porosity [%]	88.2		85.0	

Industrial scale experiments

The industrial scale experiments were done at SAPA Heat Transfers in Finspång, Sweden. The set-up of the furnace, filter, and casting table is shown schematically in Figure 3. 12 ton melt out from the holding furnace runs into the 15"×15" Drache filter after alloyed with grain refiner (Ti_5B_1 rod), and cast into one ingot. The alloy was 2wt% Si, 0.5wt% Fe, 0.2 wt% Cu, 0.9wt% Mn, 0.2wt %Mg, and 0.1wt% Zn and melt temperature at the filter was about 725°C.

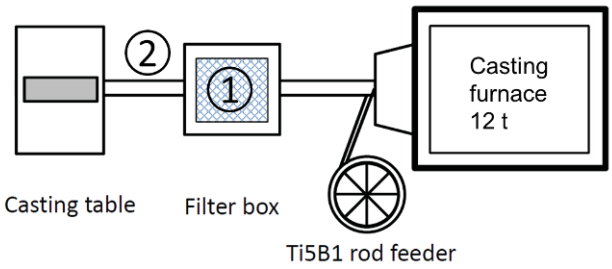

Figure 3: Filter test set-up at SAPA. LiMCA II was used to measure the inclusion content at position 1 and 2.

Initially two LiMCA II units (one on top of the filter in the filter box (Figure 3, position 1) and one after the filter box (Figure 3, position 2)) were supposed to be used to measure the inclusion content before and after the filter at SAPA. Unfortunately, only one of the units worked at the time of the experiments so that the one which was working had to be moved between position 1 and 2 during the trials.

The composition and characteristics for the filters used at SAPA are given in Table 3. Note that the SiC composition in the SiC based filter was increased to around 70% compared to the lab tested one. ``High flow`` means that the filter was designed for high flow rate metal by opening more windows in the filter.

Table 3: Composition and characteristics of the filters used in the industrial experiments.

	Al_2O_3 based filter		SiC based filter	
Composition [%]	Al_2O_3	85 – 90	Al_2O_3	≈ 6
	P_2O_5	≈ 6	SiC	≈ 70
	SiO_2	≈ 6	SiO_2	≈ 23
	$K_2O + Na_2O$	≈ 1	$K_2O + Na_2O$	0.5
Grade[ppi]	60 "High flow"		40	

Results and discussion

Lab scale experiments

Prior to each filtration test, 10 bi-film samples were taken. These were later cut, polished, and analyzed by image analysis. The results are given in Table 4. The numbers are the average and standard deviation of the sum of the diameter of pores in every sample and are given in mm. The bi-film index gives a qualitative picture of the metal purity used for the filtration tests. As seen from Table 4 tests 1 and 2 had a considerable lower bi-film index than test 3 and 4, which means a lower inclusion load of metal to be filtered.

Table 4: Bi-film index analysis of the metal used in the filtration experiments. The numbers are average with standard deviation of 10 samples for each filtration experiment.

	Inclusion load (bifilm index)
Test 1	8 ± 4
Test 2	7 ± 4
Test 3	160 ± 20
Test 4	170 ± 10

Figure 4 shows a typical test run. The preheated filters are placed in the sand mould at about time = 2.2 min. The thermocouples are

positioned about 20 mm below the filters. The metal is poured into the mould at about time = 4.3 min. The temperatures rise very rapidly to about 750°C.

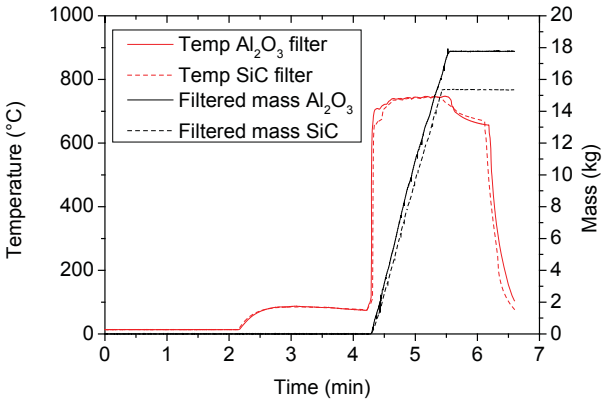

Figure 4: Typical temperature and weight curves during one parallel experiment.

In Figure 5 the weight curves during filtration for all the parallel experiments are plotted together. The total amount of melt filtered was about 17 – 20 kg through all filters

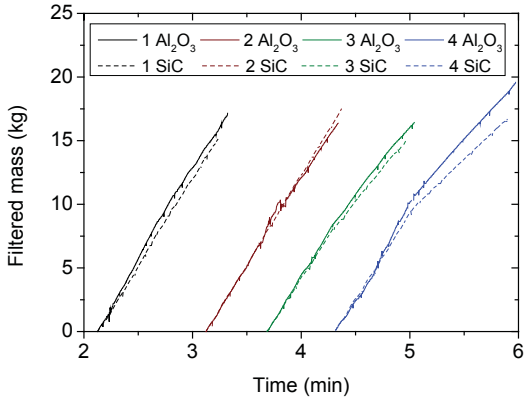

Figure 5: Weight curves versus time during the filtration period for all the parallels. The time of the start of the filter tests are shifted to an arbitrary start.

For most of the experiments there seems to be two stages where the second stage has a slower melt flow than the first stage. In Figure 6 the weight curve for 4 SiC is analyzed. According to the bi-film counting as shown in Table 4, the aluminium used in this test was one of the most dirty ones. The uncertainty in the slopes are also given in the figure. These uncertainties were all much smaller than 1% (relative to slope value) and are disregarded in the following discussion.

The slopes of all the weight curves were analyzed and the results are presented in Figure 7.

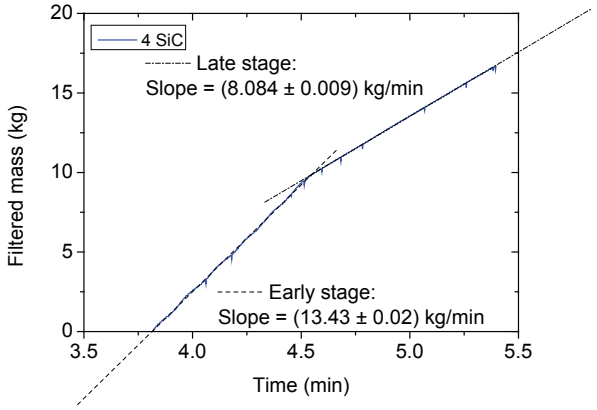

Figure 6: Analysis of the weight curve from test number 4 with SiC-based filter.

The early stage seems not to be affected by the inclusion load. However, the flow through the SiC-based filters is somewhat slower than through the Al_2O_3-based filters. This may indicate that the SiC-based filter collects more films and therefore restricts the flow more than the Al_2O_3-based filter. Another explanation is that even though the filters were produced in the same production line, they might have different inherent flow restriction due to difference in the slurries they were made of.

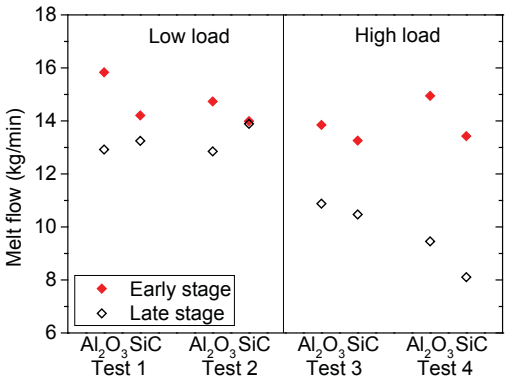

Figure 7: Slopes of the weight curves during all the filtration tests. The left part contains the two experiments with the low inclusion load, and the right side the two with high inclusion load.

For the high load experiments the melt flow is significantly decreased after some time. This is most probably a result of partially clogging of the filter at the inlet due to the collected films. According to filtration theory, while particles and films are collected inside the filter (deep-bed mode), the mass of filtered metal as function of time should be linear (as it is) [6]. Later, as a cake is forming at the inlet of the filter, the filtered mass should be proportional to $t^{1/2}$ because of a constant built-up of a pressure drop above the filter. In the parallel experiments the mass versus time was linear also after the transition. One explanation for the observed trend is that the film was not evenly distributed in the melt during the filtration tests. In other words, there were very little particles in the melt after the transition. One other explanation is that the theory which gives the $t^{1/2}$-dependency assumes a non-compressible filter-cake; that is the flow resistance in the filter-

cake is linearly dependent on the thickness of the cake and constant over time. This assumption might not hold in these experiments where the inclusions are in the form of relatively large films.

It has also been investigated when the transition from fast to slow melt flow (early to late stage) appeared. That is, how much metal had gone through the filter when the metal flow started to be slower? The result is shown in Figure 8 where about half of the melt had passed the filter before the transition. The transition appeared when between 8 – 11 kg of melt had passed the filter. One could expect that higher inclusion load in the liquid melt would lead to an earlier transition. This was not found.

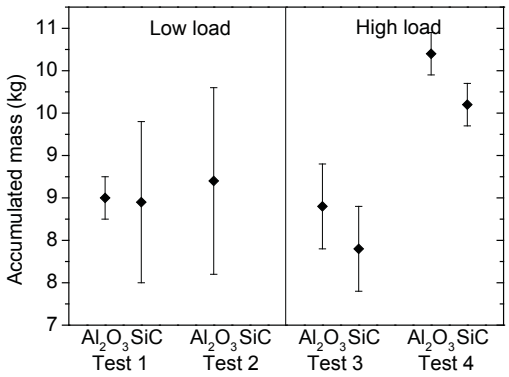

Figure 8: Transition point for the early to late stages of metal flow through the filters. No transition was found for the SiC-based filter in test number 2.

The measured temperatures below the filter are shown in Figure 9. There is no significant difference between the SiC and Al_2O_3 based filters with respect to the temperatures. There is also small temperature difference between the four tests (from 730° – 750°C).

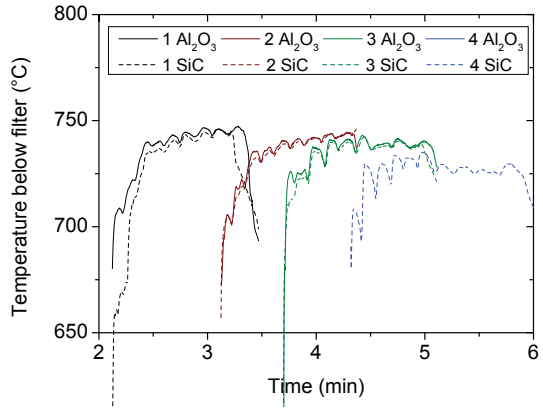

Figure 9: Temperature below the filters versus time during the filtration period for all the parallels. The thermocouple below the alumina-based filter in the fourth experiment was not working.

After the filters were used, they were cut through the middle plane along the flow direction. The cut planes were polished and an array of micrographs was taken from every filter sample. One example of a micrograph is shown in Figure 10. All the micrographs from all the filters were analyzed by image analysis.

Figure 10: Micrograph from an inlet of a filter. The oxide films are clearly seen and are up to several mm long.

As expected, far most of the films were collected at the inlet part of the filters. About 10 mm down into the filter very few films were found.

The total length of films collected per kg metal is shown in Figure 11. All the filters in two tests with the dirtiest melt (number 3 and 4) seem to collect more films than the two other tests (1 and 2). For test number 1, 2, and 3, the SiC-based filter collected more films than the Al_2O_3 based filter. For test number 4, the situation is reversed where the Al_2O_3-based filter collected more films. No explanation has been found for the behavior of the two filters in test number 4. It might be that the filter preparation and image analysis of these filters were not the same as for the others even though the same persons did the same work with all the filter samples.

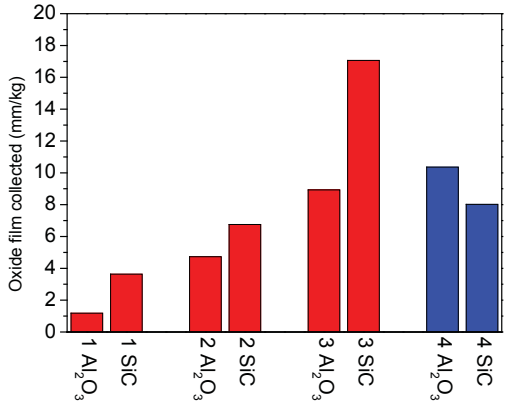

Figure 11: Total oxide film length collected per kg of metal filtered for all the experiments. The test number four has a different colour because it differs from the others.

Industrial scale experiments

As described in the experimental section, LiMCA II was used to measure the melt quality before and after the filter. Figure 12 and Figure 13 show the average number size distribution and removal efficiency as function of size for the two industrial tests at SAPA. The removal efficiency as function of particle size is defined as

$$E = 1 - \frac{N_{out}}{N_{in}} \qquad (1)$$

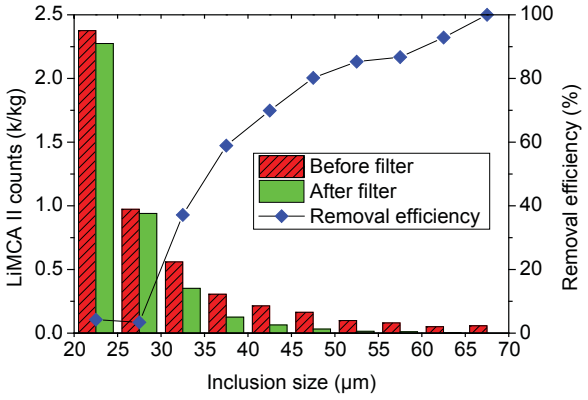

Figure 12: Average number size distribution in and out of the Al_2O_3 based filter. The blue curve shows the average removal efficiency.

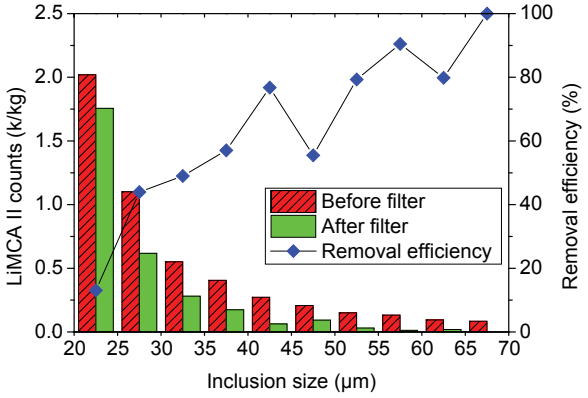

Figure 13: Average number size distribution in and out of the SiC based filter. The blue curve shows the average removal efficiency.

A recent published work shows that one way to utilize the LiMCA II data is to take into account the settling of inclusions in the furnace during the time of filtration [1]. Due to difference in density between particles and melt, the number of particles will change with time. The size distribution of the inclusions will also change during this settling time since larger inclusions will settle faster than smaller ones which is easily seen from Stokes' settling law:

$$v_s = \frac{g(\rho_p - \rho)}{18\mu} D_p^2 \qquad (2)$$

Therefore, in order to quantitatively describe the removal efficiency we have to study a narrow size range. From an industrial point of view, we should study the largest particles since they are more harmful to the final product. However, we will use the small size range (20 – 25µm) since the number of these are high enough to get reasonable statistical significance.

From equation (2) it can also be derived that the particle concentration as function of time for a given particle size will follow an exponential decreasing function:

$$N(t) = \exp(a - b \cdot t) \qquad (3)$$

where a and b are positive constants, but dependent on the inclusion size.

This applies both for the inlet concentration and outlet concentrations. By fitting curves as in equation (3) to the inlet and outlet concentrations and extrapolating the curves backward and forward in time respectively it is possible to calculate the removal efficiency as function of time from the start of LiMCA II measurements until the end.

At the time of a LiMCA II measurement the uncertainty in removal efficiencies is calculated with the use of 68% confidence limits while for the extrapolated time curve the 68% prediction limits are used. The reason for using the 68% limits as uncertainties is that this is equivalent to using ± 1 standard deviation for normally distributed populations [7].

The uncertainty in the removal efficiency is derived from equation (1) to be [8]

$$\Delta E = (1 - E)\sqrt{\left(\frac{\Delta N_{out}}{N_{out}}\right)^2 + \left(\frac{\Delta N_{in}}{N_{in}}\right)^2} \qquad (4)$$

Where ΔN_{out} is given by the 68% confidence limits within the time span N_{out} was measured and the 68% prediction limit outside the same time span, with the symmetrical procedure for ΔN_{in}.

In Figure 14 and Figure 15 the 20 – 25µm inclusion density as function of time for the Al_2O_3 and SiC based filter tests are shown respectively. Also the removal efficiencies with uncertainties are plotted with scale on the right hand axis. The measurements which are grey are all disregarded in the fitting of the time curves. This is justified since at that time the casting furnace is tilted so much that some particles which earlier have settled, start to be re-entrained in the metal flow out into the filter.

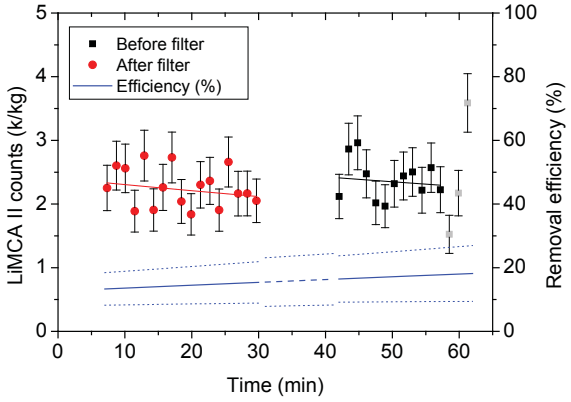

Figure 14: LiMCA II measurements and filtration efficiency for 20 – 25 µm inclusions during the test at SAPA using a 60 ppi "High flow" Al_2O_3 based filter.

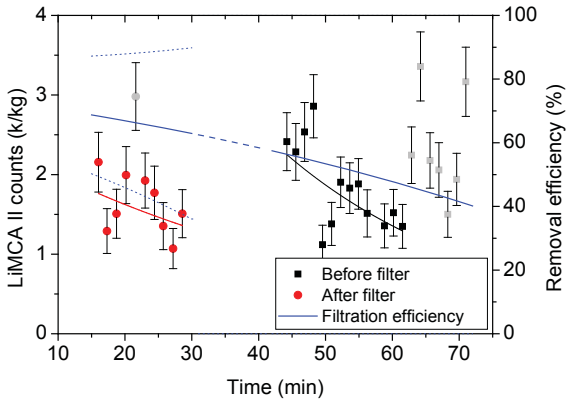

Figure 15: LiMCA II measurements and filtration efficiency for 20 – 25 µm inclusions during the test at SAPA using a 40 ppi SiC based filter.

There seems to be two main differences between the performance to the Al_2O_3 and the SiC-based filters. First the removal efficiency decreases for the SiC-based filter whereas there is a slight increase in the filtration efficiency as function of time for the Al_2O_3-based filter. Secondly the removal efficiency is generally higher in the SiC-based filter than in the Al_2O_3-based filter. This in spite of that the Al_2O_3-based filter is a 60 ppi filter and the SiC-based filter 40 ppi filter. These results are supported by the lab-scale experiments where the SiC-based filter collected more films than the Al_2O_3-based filter.

On the other hand, one should be careful to conclude too much out of only two industrial measurement campaigns. The scatter in the measurements are large, and thus also the uncertainties in the calculated removal efficiencies. For time > 30 min in Figure 15 the calculated 68% uncertainties extends from 0 to 100%.

Conclusion

A set-up for parallel testing of two different filter materials has been designed. The filter experience the same pressure drop and the same inclusion load while the melt flows through each filter are recorded separately.

It was found that for most of the tests, the melt flow through the filters experience a shift during the tests. That is, at some stage the melt flow decreased significantly. The flow through the SiC-based filter is reduced more than through the Al_2O_3-based filter for high inclusion load.

Image analysis of the used filter showed that in most cases the SiC-based filter collected more films than the Al_2O_3-based filter. This is in accordance with the industrial measurements and calculated removal efficiencies from the LiMCA II data where the removal efficiency in the SiC-based filter is higher than in the Al_2O_3-based filter.

From the LiMCA II measurements in the industry trials, there seems to be a decreasing trend for the removal efficiency in the SiC-based filter while the removal efficiency increased in the Al_2O_3-based filter. However, the removal efficiency in the SiC-based filter was always higher than in the Al_2O_3-based filter.

Acknowledgements

This research was partly carried out as part of the Norwegian Research Council (NRC) funded BIP Project (No. 179947/I40) RIRA (Remelting and Inclusion Refining of Aluminium), and partly the RCN funded BIA Project No. 219940/O30 Quality Aluminium Cast House (QuAlity). They include the partners: Hydro Aluminium AS, SAPA Heat Transfer AB, Alcoa Norway ANS, NTNU and SINTEF. Fundings by the industrial partners and NRC is gratefully acknowledged. Hydro Aluminium Profiler AS at Raufoss is also acknowledged for supplying the anodized profiles while Drache is acknowledged for supplying the filters.

References

1. M. Syvertsen, S. Bao, T. Engh, A. Kvithyld, *Performance Evaluation of Two Different Industrial Foam Filters with LiMCA II Data.* Metallurgical and Materials Transactions A, 2013. Accepted.
2. S. Bao, K. Tang, A. Kvithyld, M. Tangstad, T.A. Engh, *Wettability of Aluminium on Alumina.* Metallurgical and Materials Transactions B, 2011. 42(6): p. 1358-1366.
3. S. Bao, *Filtration of aluminium -experiments, wetting and modelling*. PhD Thesis. 2011, Norge s teknisk-naturvitenskapelige universitet: Trondheim. p. 204 s.
4. S. Bao, M. Syvertsen, A. Nordmark, A. Kvithyld, T. Engh, M. Tangstad, *Plant Scale Investigation of Liquid Aluminium Filtration by Al $_2O_3$ and SiC Ceramic Foam Filters* , in *TMS*. 2013.
5. D. Dispinar, A. Kvithyld, A. Nordmark, *Quality Assesment of Recycled Aluminium.* Light Metals, 2011: p. 731-735.
6. T.A. Engh, *Principles of Metal Refining* . 1992: Oxford University Press. 61.
7. W.H. Press, *Numerical Recipes 3rd Edition: The Art of Scientific Computing*. 2007: Cambridge university press.
8. G.L. Squires, *Practical Physics*. 1985, Cambridge: Cambridge University Press. xii, 215 s.